An integrated prognostics approach for pipeline fatigue crack growth prediction utilizing inline inspection data

Mingjiang Xie[1], Steven Bott[2], Aaron Sutton[2], Alex Nemeth[2], Zhigang Tian[1*]

[1] Department of Mechanical Engineering, University of Alberta, Edmonton, AB, Canada

[2] Enbridge Liquid Pipelines, Edmonton, AB, Canada

Abstract

Fatigue cracking is a key type of defect for liquid pipelines, and managing fatigue cracks has been a top priority and a big challenge for liquid pipeline operators. Existing inline inspection (ILI) tools for pipeline defect evaluation have large fatigue crack measurement uncertainties. Furthermore, current physics-based methods are mainly used for fatigue crack growth prediction, where the same or a small range of fixed model parameters are used for all pipes. They result in uncertainty that is managed through the use of conservative safety factors such as adding depth uncertainty to the measured depth in deciding integrity management and risk mitigation strategies. In this study, an integrated approach is proposed for pipeline fatigue crack growth prediction utilizing inline inspection data including consideration of crack depth measurement uncertainty. This approach is done by integrating the physical models, including the stress analysis models, the crack growth model governed by the Paris' law, and the ILI data. With the proposed

integrated approach, the finite element (FE) model of a cracked pipe is built and stress analysis is performed. ILI data is utilized to update the uncertain physical parameters for the individual pipe being considered so that a more accurate fatigue crack growth prediction can be achieved. Time-varying loading conditions are considered in the proposed integrated method by using rainflow counting method. The proposed integrated prognostics approach is compared with the existing physics based method using examples based on simulated data. Field data provided by a Canadian pipeline operator is also employed for the validation of the proposed method. The examples and case studies in this paper demonstrate the limitations of the existing physics-based method, and the promise of the proposed method for achieving accurate fatigue crack growth prediction as continuous improvement of ILI technologies further reduce ILI measurement uncertainty.

1 Introduction

Pipelines are known as being the safest and most economical way to transport large quantities of oil and gas products. According to the Canadian Energy Pipeline Association (CEPA), 94% of the refined petroleum products, and most of the Canadian oil and gas exports were transported by pipelines [1]. Pipelines are subject to different types of defects, such as fatigue cracking, corrosion, etc. [2], [3], [4]. Without proper remediation actions, these defects can eventually result in pipeline failures including leaks or ruptures, which lead to public safety issues, i.e. a release of pipeline contents to the environment, and expensive downtime. ILI runs are performed periodically using

smart pigging tools to detect defects and evaluate pipeline health conditions. Fatigue cracking refers to crack growth due to fatigue caused by pressure cycling during pipeline operations.

Fatigue cracking is a key type of defect for liquid pipelines, and managing such fatigue cracks continues to be a top priority amongst pipeline integrity management. However, existing ILI tools have relatively large fatigue crack measurement uncertainties, and typically have a specification of about plus/minus 1 millimeter, 80% of the time [2], [5]. Furthermore, currently physics-based methods are mainly used for fatigue crack growth prediction, based on crack growth models governed by the Paris' law [5], [6]. The uncertainty in crack sizing and the Paris' law model grows to the predicted time of failure due to fatigue cracks, resulting in uncertainty which requires a conservative management integrity management approach and risk mitigation strategies, such as repairs, pipe replacement, pressure reductions and hydro-testing. There is an urgent need to develop accurate fatigue crack growth prediction tools, and reduce the uncertainty and hence the conservatism in pipeline integrity management.

Existing pipeline defect prognosis methods are mainly classified into physics-based methods and data-driven methods[7]. The physics based methods for pipelines mainly include stress-life method (*S*-*N*), local strain method (*ε*-*N*), and Paris' law based methods [8]. Among them, the physics-based method governed by the Paris' law is currently the dominant method used for pipeline fatigue crack growth prediction [2,5,6]. The Paris'

law is generally used for describing fatigue crack growth [5], [6], [9], [10]:

$$\frac{da}{dN}=C(\Delta K)^m \tag{1}$$

where da/dN is the crack growth rate, a is crack size, N is the number of loading cycles, ΔK is the range of the Safety Intensity Factor (SIF), and C and m are material related uncertainty model parameters. C and m can be estimated via experiments, and are set as fixed constants in the physics-based method. Many studies have been published on using physical models, such as FE models, and crack growth models based on *S-N* curves or some forms of Paris' law. Hong et al. [11] estimated the fatigue life by using the *S-N* curves of the ASTM standard specimens, curved plate specimens and wall-thinned curved plate specimens. Pinheiro and Pasqualino [12] proposed a pipeline fatigue analysis based on a finite element model and S-N curve with the validation of small-scale fatigue tests. Oikonomidis et al. [13,14] predicted the crack growth through experiments and simulation based on a strain rate dependent damage model (SRDD). Crack arrest length and velocity can be predicted through the proposed model. A key disadvantage of the existing physics-based method is that typically the same fixed model parameters are used for all pipes (i.e. m=3). However, these material dependent model parameters should be different for different pipes, and slight differences in such model parameters can lead to large differences in fatigue crack growth predictions. As an example, a 10% change in parameter m may lead to a change of 100% in the predicted

failure time.

Data-driven methods use the experimental data or monitoring data rather than physical models for prognosis. Varela et al. [15] discussed major methodologies used to produce condition monitoring data. Among these pipeline inspection techniques, inline inspection tools are the most reliable for pipeline integrity management. A review of ILI tools for detecting and sizing cracks was conducted in reference [16]. Slaughter et al. [17] analyzed the ILI data for cracking and gave an introduction to how to improve the crack sizing accuracy. Systematic error of the ILI tool, measurement noise and random error from the tool, and the surface roughness are three main sources of ILI tool uncertainties [18]. Due to the measurement errors and cost of an ILI tool, data driven methods do not work well if the number of ILI tool runs and the amount of data are not sufficient.

In this paper, an integrated approach for pipeline fatigue crack growth prediction with the presence of large crack sizing uncertainty is proposed, which integrates the physical models and the ILI data. With the proposed integrated approach, the FE model of cracked pipe is built and stress analysis is performed. ILI data is employed to update the uncertain material parameters for the individual pipe being considered so that a more accurate fatigue crack growth prediction can be achieved. The proposed integrated approach is compared with the existing physics based method using examples based on simulated data. Field data provided by a Canadian pipeline operator is also used to validate the proposed integrated approach.

Time-varying operating conditions are considered in the proposed integrated method. When oil and gas content is transported with pipelines, the internal pressure of the operating pipelines varies with time, which presents a challenge for applying integrated prognostics methodology. Zhao et al. [19] proposed an integrated prognostics method for a gear under time-varying conditions. The load changes history considered in [19] is the combination of several constant loading conditions, while in pipeline operations, the internal pressure changes continuously. In this study, we employ the rainflow counting method to deal with time-varying operating conditions. A key advantage of using the rainflow counting method within the proposed integrated method is to directly link the environmental and human factors which affected the loading conditions to the degradation model. Also, it is proven by Roshanfar and Salimi [20] that rainflow counting method is more accurate compared with other cycles counting methods, such as range counting, level crossing counting, and peak counting methods.

Section II presents a pipe element model considering a single fatigue crack. The proposed integrated method for fatigue crack growth prediction of pipeline is discussed in Section III. Section IV gives examples based on simulated data and Section V presents a case study to demonstrate the proposed method. Section VI gives the conclusions.

2 Pipe finite element modeling considering fatigue cracks

In this section, the pipe finite element model considering a single fatigue crack is built, based on information and methods presented in [21–23]. The ANSYS software is used for pipe FE modeling, and a single semi-elliptical type of crack is considered. Stress analysis is performed, and SIF can be calculated.

2.1 Pipe FE modeling

Test data 157-1 presented in Reference [24] on line pipes was used. The material is X70 grade pipe steel. Table 1 shows the line pipe's physical properties.

Table 1 Physical properties of the line pipe

API 5L Grade	X70
Yield Strength Min. (MPa)	483
Tensile Strength Min. (MPa)	565
Yield to Tensile Ratio Max.	0.93
Elongation Min.	17
Outside Diameter (mm)	914.4
Wall Thickness (mm)	15.875
Length (mm)	5000
Internal Pressure (MPa)	10

Software ANSYS Workbench is used to build the FE model. The crack shape is set to Semi-Elliptical, which is the most common type of fatigue cracks found in pipelines. The

crack size and shape are defined by the major radius (crack length a=2r) and the minor radius (crack depth b), which are shown in Fig. 1. ANSYS Workbench was used to build a pipeline model with a semi-elliptical crack, with the input of major radius and minor radius.

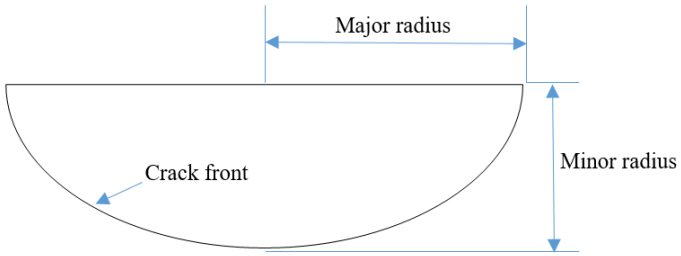

Fig. 1 Crack Shape

The pipe parameters are entered using the fracture tool. The pipe is divided into two parts: one is the fracture affected zone which uses the tetrahedrons method, and the other is the rest of the pipe which uses the hex-dominant method. Fig. 2 shows the built FE model, where the base mesh without cracks and the region involving the crack are modeled using the two different modeling methods.

Stress intensity factor (SIF) is the key output of pipe finite element analysis. The crack length a increases from 4mm to 30mm with a step size of 2mm, and the crack depth b is varied from 2mm to 12mm with 1mm increments, and obtain the corresponding SIF values through stress analysis. To model the relationship between SIF values at the surface point (K_a), at the deepest point (K_b), along with the crack length and depth, a curve fitting tool with polynomial function in Matlab was used. The results are

presented in Fig. 3. The curve fitting results show that the two adjusted R-squares are both very close to 1, indicating good goodness of fit.

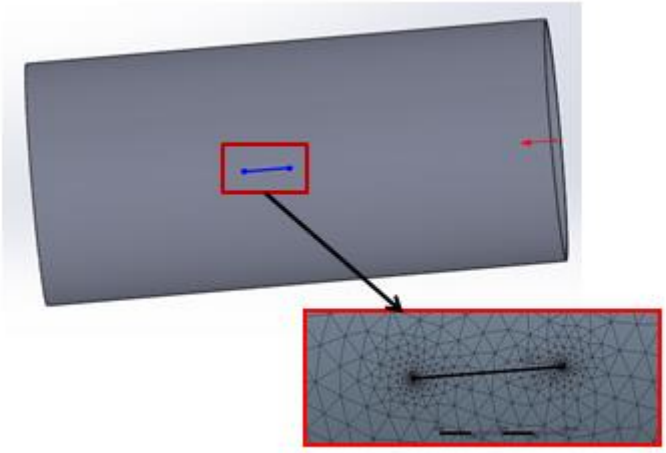

Fig. 2 Crack built in ANSYS workbench

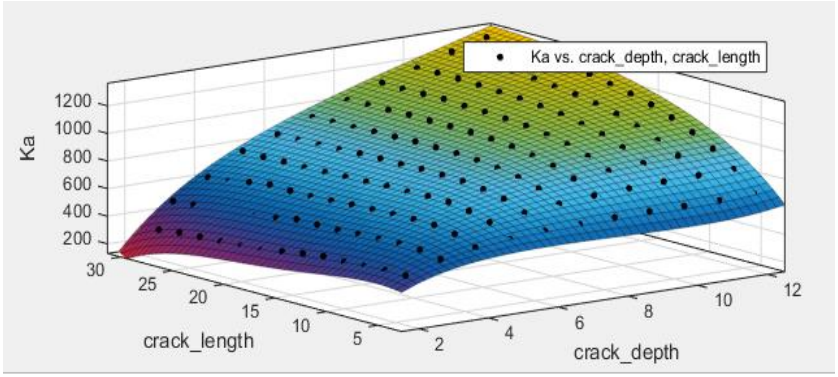

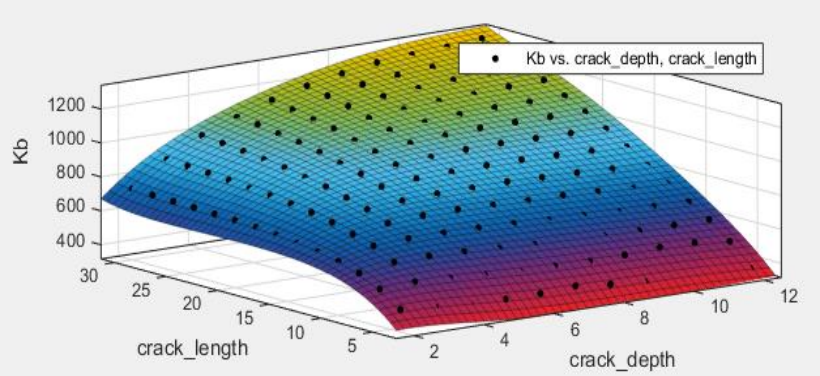

Fig. 3 The fitted SIF functions

The internal pressure is varied from 0.69MPa to 2.76MPa in 0.69Mpa increments to find the SIF values at the surface point and those at the deepest point, which are displayed in Table 2. It can be concluded that the SIF is proportional to pressure. It can also be verified through the technique by Raju and Newman [25], which is widely applied to evaluate pipe stress considering fatigue cracks:

$$\Delta K=\Delta\sigma f\sqrt{\pi\frac{a}{Q}}=\Delta P\frac{D}{2t}f\sqrt{\pi\frac{a}{Q}} \tag{2}$$

where $\Delta\sigma$is the range of the hoop stress, ΔP is the size of the pressure cycle, a is the instantaneous crack depth, and f and Q are constants that depend on pipe geometry and defect length, respectively. Given that SIF is proportional to pressure, the SIF can be calculated at a certain pressure to obtain the SIF value at a different pressure by scaling the SIF value proportional to the pressure level [19].

Table 2 Pressure influence on SIF

P(MPa)	a(mm)	b(mm)	K_a	K_b
0.69	15.2	2.54	653.36	1187.6
1.38	15.2	2.54	1306.7	2375.2
2.07	15.2	2.54	1960.1	3562.7
2.76	15.2	2.54	2613.4	4750.3
0.69	15.2	5.08	1193.6	2340.9
1.38	15.2	5.08	2387.1	4681.9
2.07	15.2	5.08	3580.7	7022.8
2.76	15.2	5.08	4774.3	9363.8
0.69	50.8	5.08	792.33	2219.7
1.38	50.8	5.08	1584.7	4439.4
2.07	50.8	5.08	2377	6659
2.76	50.8	5.08	3169.3	8878.7

2.2 Pipe FE model verification

The pipe FE model is partially verified by comparing with the Raju and Newman method [25], outlined in "OPS TTO5 – Low Frequency ERW and Lap Welded Longitudinal Seam Evaluation" [26]. The Raju and Newman method for calculating SIF for a semi-elliptical surface flaw is implemented in this project based on the following equations (3-8).

$$\Delta K=\Delta\sigma f\sqrt{\pi\frac{a}{Q}}=\Delta P\frac{D}{2t}f\sqrt{\pi\frac{a}{Q}} \tag{3}$$

where:

$$Q=1+4.595\left(\frac{a}{L}\right) \tag{4}$$

$$f=M_1+M_2\left(\frac{a}{t}\right)^2+M_3\left(\frac{a}{t}\right)^4 \tag{5}$$

$$M_1=1.13-0.18\left(\frac{a}{L}\right) \tag{6}$$

$$M_2=\frac{0.445}{0.1+\frac{a}{L}}-0.54 \tag{7}$$

$$M_3=0.5-\frac{0.5}{0.325+\frac{a}{L}}+14\left(0.5-2\left(\frac{a}{L}\right)\right)^{24} \tag{8}$$

ΔP is the size of the pressure cycle, a is the depth of crack from the pipe surface, L is the length of the crack, D is outside diameter, and t is the pipe wall thickness.

The results by the Raju & Newman's method are compared with those obtained using the FE model, when the flaw length is 150mm (5.9in.). 150mm (5.9in.) is used

because it corresponds to the case study in Section 5.The two curves are shown in Fig. 4. As can be observed, the values calculated using these two methods are pretty close for a large portion of the crack depth range. The FE method is also compared with two other methods for cracked pipe SIF calculations: API 579 and BS 7910, which are outlined in Section 4.

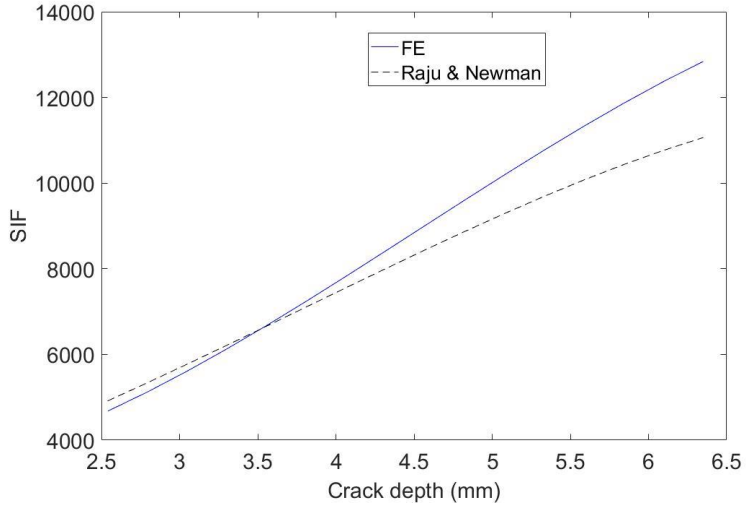

Fig. 4 Comparison of SIF results between the Raju & Newman method and the FE method

3 The proposed integrated method for fatigue crack growth prediction

In the proposed integrated method for fatigue crack growth prediction, the pipe FE model calculates the SIF values for given crack sizes, which are utilized in the crack growth model governed by the Paris' Law for propagating the fatigue. The distributions

of the uncertain model parameters are updated through Bayesian approach using the current fatigue crack size [27]. The estimate is based on ILI or nondestructive evaluation (NDE) data to get the uncertain model parameters to approach the real values for the specific unit being monitored. With the updated uncertain model parameters, the crack growth model can be applied to predict future crack growth and subsequently the failure time distribution. As part of the proposed approach, the pipe FE models are described in Section 2, and can be used for SIF computation.

3.1 Crack growth model

The fatigue propagation of a semi-elliptical surface crack considering two crack growth directions was analyzed. Newman and Raju [25] indicate that the aspect ratio change of surface cracks should be calculated by assuming that a semi-elliptical profile is always maintained, and that it is adequate to use two coupled Paris fatigue laws known as “two-point plus semi-ellipse” method:

$$\frac{da}{dN} = C_A(\Delta K_A)^{m_A} \tag{9}$$

$$\frac{db}{dN} = C_B(\Delta K_B)^{m_B} \tag{10}$$

where ΔK_A and ΔK_B are the ranges of the stress intensity factor at the surface points and the deepest point of the surface crack, and C_A, C_B, m_A and m_B are material constants.

The simulated crack growth paths using the evolution equations considering C_A=C_B, m_A= m_B is more in accordance to the actual fatigue tests results reported in [28]. A semi-elliptical crack can propagate to a new semi-elliptical one based on the "two-point plus semi-ellipse" method [29,30].

3.2 Bayesian inference for uncertain model parameter updating

In this section, the degradation model adopts two basic coupled Paris' law formulas as the crack growth model. On the right-hand side of the formula, a model uncertainty term ε is added to make the propagation model more accurate. The modified Paris' law can be represented by the following equations after considering the model uncertainty:

$$\frac{da}{dN}=C(\Delta K_A)^m\varepsilon \tag{11}$$

$$\frac{db}{dN}=C(\Delta K_B)^m\varepsilon \tag{12}$$

In addition, we assume that the measurement error $e=a_{real}-a_{meas}=b_{real}-b_{meas}$ has the following distribution

$$e\sim N(0,\sigma^2) \tag{13}$$

The measured crack length and crack depth a_{meas}, b_{meas} follow normal distributions centered at a_{real}, b_{real} as follows:

$$a_{meas}\sim N(a_{real},\sigma^2) \tag{14}$$

$$b_{meas} \sim N(b_{real}, \sigma^2) \quad (15)$$

In physics-based methods, researchers use physical models for prognostics without considering the uncertainty of ILI data. In some papers, they only used the ILI data as a new starting point instead of updating model parameters of physics-based models. In this paper, ILI data is used to update the uncertain material parameters using the Bayesian inference method. Because parameter *m* affects the degradation path and the predicted results more than parameter *C* based on the Paris's law, only the distribution of m is updated, while maintaining other model parameters unchanged. Thus, the posterior distribution $f_{post}(m|a,b)$ can be obtained through the Bayesian inference method:

$$f_{post}(m|a,b) = \frac{l(a,b|m) f_{prior}(m)}{\int l(a,b|m) f_{prior}(m) \mathrm{d}m} \quad (16)$$

where $f_{prior}(m)$ represents the prior distribution of m; $l(a,b|m)$ represents the probability of detecting measured crack sizes, including length *a* and depth *b*.

Paris' law is employed to propagate the crack from the current ILI measured crack size to the ones at next inspection point with given value of *m*. Due to uncertainties in ILI tool and Paris' law, there exists the possibility to detect a certain crack length and crack depth at the next inspection point. The possibility can be denoted by a likelihood function $l(a,b|m)$.

3.3 The integrated method considering crack depth only

In most cases, the pipe fatigue crack does not propagate much along the crack length direction. If only growth along the crack depth direction is considered, the Paris' law model can be simplified to [31]:

$$\frac{\mathrm{d}a}{\mathrm{d}N}=C(\Delta K)^{m}\varepsilon \tag{17}$$

And the equation for Bayesian updating is:

$$f_{\text{post}}(\mathrm{m}\,|\,\mathrm{a})=\frac{l(a/m)f_{\text{prior}}(m)}{\int l(a/m)f_{\text{prior}}(m)\mathrm{d}m} \tag{18}$$

4 Examples based on simulated data

4.1 Simulation example with the same starting point

In the example in this section, the proposed prognostics approach is verified based on simulated data. It is assumed that the standard deviation of ILI tool error equals to 0.15, C=5e-12, m~(2.5,0.2^2), and ε~N(0,0.2^2). We also set the initial crack length as 4mm and initial crack depth as 2mm.

Ten degradation paths are generated, as shown in Fig. 5. The ten degradation paths are obtained based on the two Paris' law formulas, one for crack length and the other for crack depth, based on the above-mentioned model parameters. The initial crack length and depth are the same for all the ten degradation paths. The generated paths

are separated into two sets: a training set, which is to derive a prior distribution of uncertain material parameter *m*, and a test set. The prediction performance of the proposed approach can be evaluated based on the test set.

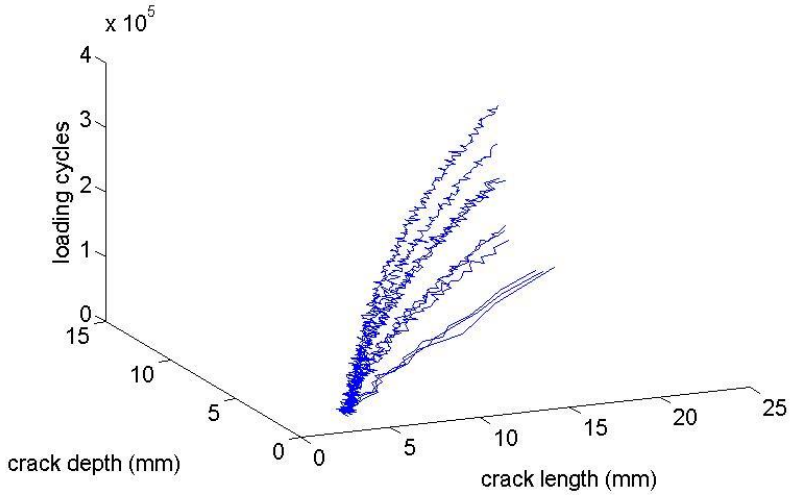

Fig. 5 Ten simulated degradation paths

We select path 1 to 5 as the training set and 6 to 10 as the test set. Table 3 shows the ten real *m* values, since these real values are known during the simulated degradation path generation process. For the five degradation paths in the training set, a procedure based on least-square optimization, which was reported in Ref. [9], are used to estimate the *m* value for each training degradation path. These trained *m* values are subsequently used to fit the prior distribution parameters. We select normal distribution to fit them and the prior distribution of *m* is:

$$f(m)=N(2.5439,0.1557^2) \quad (19)$$

Paths #6, #7, #8 are selected for testing the prediction accuracy of the proposed prognostics approach. During the updating process, the posterior distribution of *m* will serve as the prior distribution to update parameter *m* at the next inspection point. In path #6, a total of 2.4×10^4 cycles are taken to meet the failure criteria. All useful information in the updating process for path #6 is shown in Table 4. In path #7, the failure time is 3.1×10^4 cycles, and it is 2.8×10^4 cycles for path #8. The updating histories for mean and standard deviation values of parameter m in path #7 and path #8 are shown in Tables 5 and 6, respectively. The results show that for all these paths, their material parameter *m* is gradually updated from prior distribution to approach its own unique real value. Fig. 6 shows the plots for updated distribution of parameter *m* for path #6. The plots for updated distribution of predicted failure time for path #6, #7, #8 are shown in Figs. 7, 8, and 9, respectively.

As can be seen from the results, the updated *m* values can approach the real *m* values through updating using the observed data. The failure time predictions also approach the real failure times. The uncertainty is reduced during the updating processes.

Table 3 The real values and trained values of *m*

Path#	Real m	Trained m
1	2.3888	2.3890
2	2.5968	2.5968
3	2.7886	2.7838
4	2.4787	2.4792
5	2.4667	2.4662
6	2.8027	-
7	2.7588	-
8	2.7805	-
9	2.5850	-
10	2.5447	-

Table 4 Validation results with path #6 (real *m*=2.8027)

Loading cycles	Crack length(mm)	Crack depth(mm)	Mean of *m*	Std of *m*
0	4	2	2.5439	0.1557
0.6×10^4	5.4811	2.9010	2.7854	0.0358
1.2×10^4	7.6330	4.4793	2.7925	0.0148
1.8×10^4	11.9190	7.3864	2.8001	0.0069
2.4×10^4	22.6406	13.4753	2.8040	0.0036

Table 5 Validation results with path #7 (real *m*=2.7588)

Loading cycles	Crack length(mm)	Crack depth(mm)	Mean of *m*	Std of *m*
0	4	2	2.5439	0.1557
0.7×10^4	5.1763	2.8022	2.7239	0.0477
1.4×10^4	6.8845	4.0574	2.7428	0.0201
2.1×10^4	10.3283	6.0624	2.7617	0.0094

2.8×10^4	15.8216	9.5424	2.7546	0.0049

Table 6 Validation results with path #8 (real *m*=2.7805)

Loading cycles	Crack length(mm)	Crack depth(mm)	Mean of *m*	Std of *m*
0	4	2	2.5439	0.1557
0.7×10^4	5.3408	2.9543	2.7527	0.0382
1.4×10^4	7.5956	4.4904	2.7703	0.0152
2.1×10^4	11.8729	7.1897	2.7760	0.0072
2.8×10^4	21.7281	12.7277	2.7777	0.0035

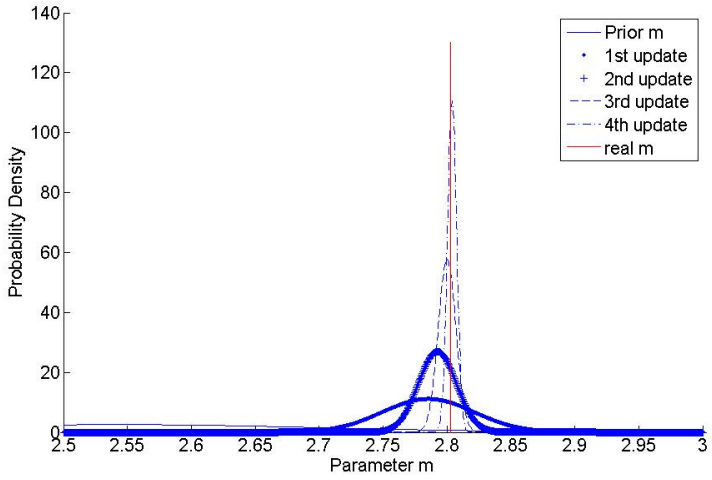

Fig. 6 Distributions of parameter *m* for path #6

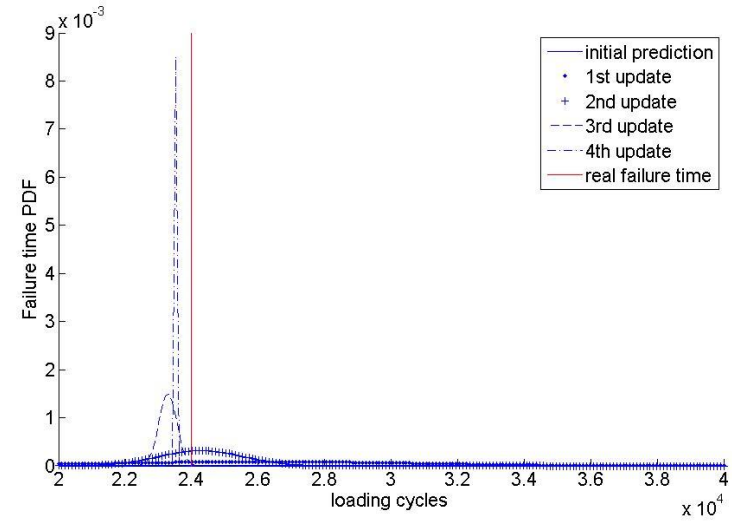

Fig. 7 Distributions of predicted failure time for path #6

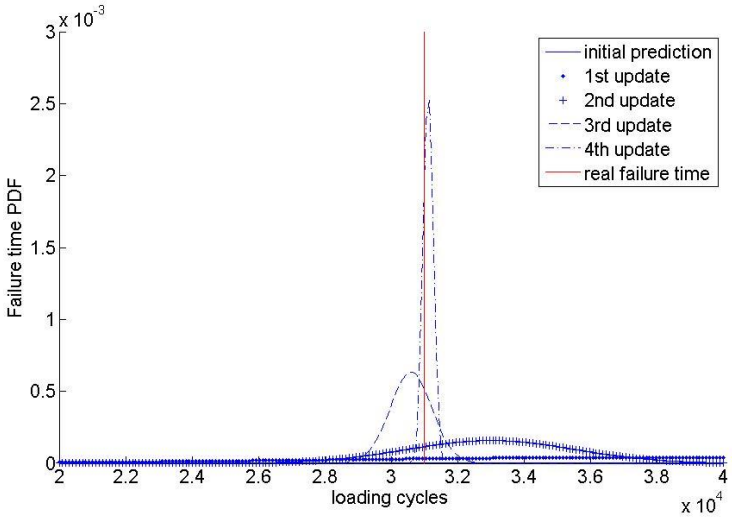

Fig. 8 Distributions of predicted failure time for path #7

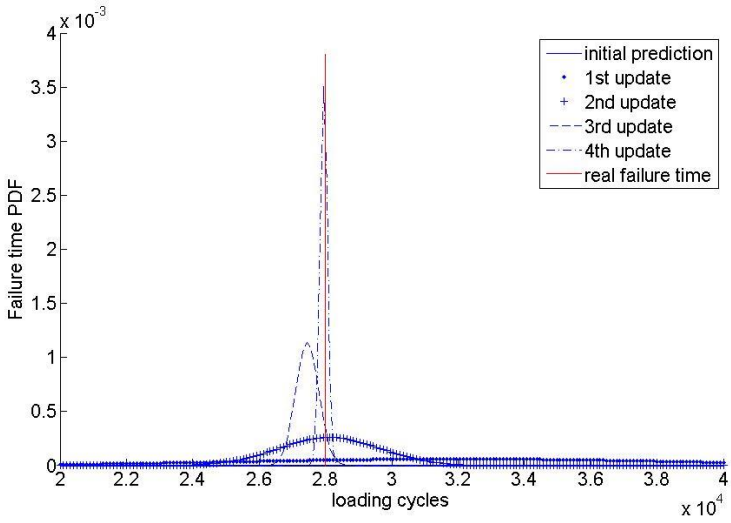

Fig. 9 Distributions of predicted failure time for path #8

4.2 Sensitivity analysis

In this section, we study the sensitivity of the results to the variation of the initial crack sizes and the ILI tool measurement error. We use the same *m* values, as those listed in Table 3 in section 4.1, to generate the ten degradation paths, and use path #6 as the test set. We change the initial crack length a_0 and/or initial crack depth b_0 while maintaining all the other parameters unchanged. In the comparison, three scenarios are considered, where initial crack length is much bigger than crack depth, much smaller than depth, or close to depth, respectively. Table 7 is then obtained with three different input sizes combinations. It should be noted that in each of the three initial crack size scenarios in Table 7, the initial crack sizes are the same for all the 10 paths in this sensitivity analysis. From the comparison results in Table 7, we can find that if we use the same inspection interval, the inspection times decrease from four times to two

times or one time, as crack lengths and/or depths increase. However, even with shorter inspection times, the mean values of *m* are all approaching the real value (2.8027), and this shows that the proposed approach works well under all these different initial conditions.

Beside initial condition analysis, we also investigate the impact of measurement errors of the ILI tools on the results. We increase σ_{ILI} from 0.15mm to 0.3mm and 0.5mm, respectively. The results are shown in Table 8. The inspection times don't change as σ_{ILI} increases. For both cases with larger measurement errors, the mean values of *m* are all approaching the real value (2.8027), which shows the effectiveness of the approach. As expected, the performance of the proposed approach becomes worse as the measurement error of ILI tool increases. This also implies that with the development of more accurate ILI tools, the lower measurement error will result in better performance for the proposed approach.

Table 7 Sensitivity analysis for initial crack depths and lengths (real *m*=2.8027)

(1) a_0=8mm, b_0=2mm

Loading cycles	Crack length(mm)	Crack depth(mm)	Mean of *m*	Std of *m*
0	8	2	2.5439	0.1557
0.6×10^4	9.8382	4.3728	2.7611	0.0383
1.2×10^4	15.1176	8.2462	2.7980	0.0110

(2) a_0=4mm, b_0=6mm

Loading cycles	Crack length(mm)	Crack depth(mm)	Mean of *m*	Std of *m*
0	4	6	2.5439	0.1557
0.6×10^4	7.1640	6.9937	2.7707	0.0342
1.2×10^4	13.9725	10.0862	2.8054	0.0096

(3) a_0=8mm, b_0=6mm

Loading cycles	Crack length(mm)	Crack depth(mm)	Mean of *m*	Std of *m*
0	8	6	2.5439	0.1557
0.6×10^4	13.9012	8.9284	2.7960	0.0121

Table 8 Sensitivity analysis for measurement errors of ILI tools (real *m*=2.8027)

(1) σ_{ILI}=0.3mm

Loading cycles	Crack length(mm)	Crack depth(mm)	Mean of *m*	Std of *m*
0	4	2	2.5439	0.1557
0.6×10^4	5.0333	3.4444	2.7343	0.0756
1.2×10^4	8.1987	4.0964	2.7958	0.0218
1.8×10^4	11.8189	7.7472	2.7988	0.0098
2.4×10^4	22.3269	12.9847	2.7985	0.0045

(2) σ_{ILI}=0.5mm

Loading cycles	Crack length(mm)	Crack depth(mm)	Mean of *m*	Std of *m*
0	4	2	2.5439	0.1557
0.6×10^4	5.1455	3.5268	2.5728	0.0847
1.2×10^4	7.4150	4.2182	2.5919	0.0450
1.8×10^4	12.9044	8.0734	2.6383	0.0258
2.4×10^4	21.7774	12.4770	2.6829	0.0133

4.3 Simulation example with different starting points

In the example in this section, we assume that the standard deviation of ILI tool error equals to 0.15, *C*=5e-12, m~(2.5,0.2^2), and ε~N(0,0.2^2), which are the same as

those in Section 4.1. The initial crack lengths and depths are uniformly random generated in the range of 4mm to 10mm, and 2mm to 6mm, respectively. In this way, we have different starting points, i.e. initial crack length and depth values, for the ten simulated degradation paths. The ten new degradation paths are generated, and shown in Fig. 10.

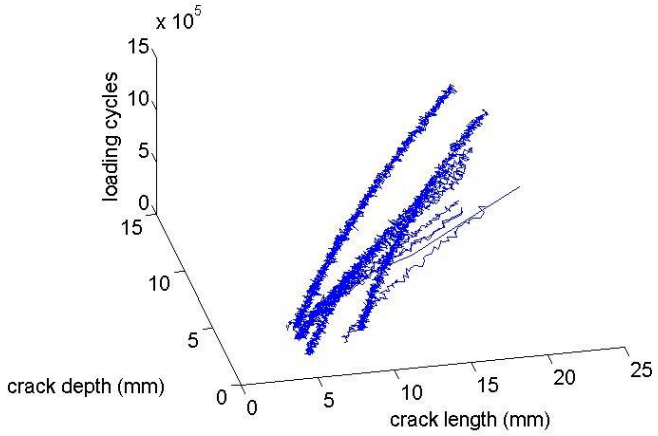

Fig. 10 Ten simulated degradation paths with different starting points

Following the same procedure as section 4.1, the real values and trained values of *m* are obtained in Table 9, and then we can obtain the prior distribution of *m* as:

$$f(m)=\mathrm{N}(2.3814,0.1352^2) \tag{20}$$

Paths #6, #7, #8 are then selected for testing the prediction accuracy of the proposed prognostics approach. In path #6, a total of 6×10^3 cycles are taken to meet the failure criteria. All useful information in the updating process for path #6 is shown in Table 10.

The updating histories for mean and standard deviation values of parameter *m* in path #7 and path #8 are shown in Tables 11 and 12, respectively. From the results in these tables, *m* is gradually updated from the prior distribution to approach its own unique real value. The plots for updated distribution of parameter *m* and predicted failure time for path #6 are shown in Figs. 11 and 12.

As can be seen from the results, the updated *m* values can approach the real *m* values through updating using the observed data. The failure time predictions also approach the real failure times. The uncertainty is reduced during the updating processes. In this example, it shows that the proposed approach works well for the case with different starting points.

Table 9 The real values and trained values of *m*

Path#	Real m	Trained m
1	2.5095	2.5096
2	2.2656	2.2653
3	2.2867	2.2864
4	2.5470	2.5468
5	2.2982	2.2979
6	2.9076	-
7	2.1310	-
8	2.3654	-
9	2.1309	-
10	2.5185	-

Table 10 Validation results with path #6 (real *m*=2.9076)

Loading cycles	Crack length(mm)	Crack depth(mm)	Mean of *m*	Std of *m*
0	5.6680	5.2929	2.3814	0.1352
2×10^3	8.1578	6.5013	2.7713	0.0161
4×10^3	11.5583	8.3144	2.8079	0.0083
6×10^3	18.3856	11.5141	2.8810	0.0011

Table 11 Validation results with path #8 (real *m*=2.3654)

Loading cycles	Crack length(mm)	Crack depth(mm)	Mean of *m*	Std of *m*
0	7.5834	5.9807	2.3814	0.1352
5×10^4	9.6401	7.2315	2.3464	0.0262
1.0×10^5	12.4980	8.3614	2.3579	0.0084
1.5×10^5	15.8673	10.3980	2.3593	0.0028

Table 12 Validation results with path #10 (real *m*=2.5185)

Loading cycles	Crack length(mm)	Crack depth(mm)	Mean of *m*	Std of *m*
0	7.0101	5.5680	2.3814	0.1352
2×10^4	9.4881	6.5740	2.5352	0.0332
4×10^4	12.0497	8.2202	2.5151	0.0137
6×10^4	15.9555	10.0877	2.5162	0.0071

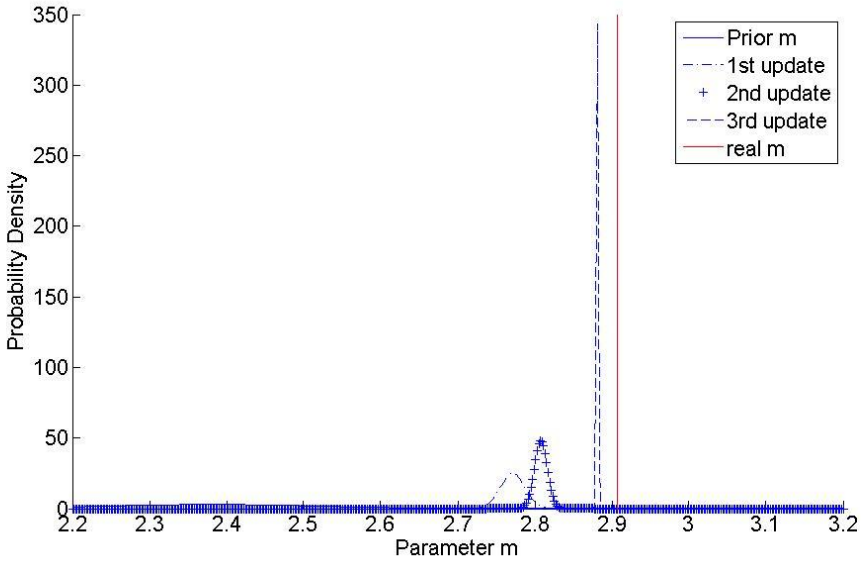

Fig. 11 Distributions of parameter *m* for path #6

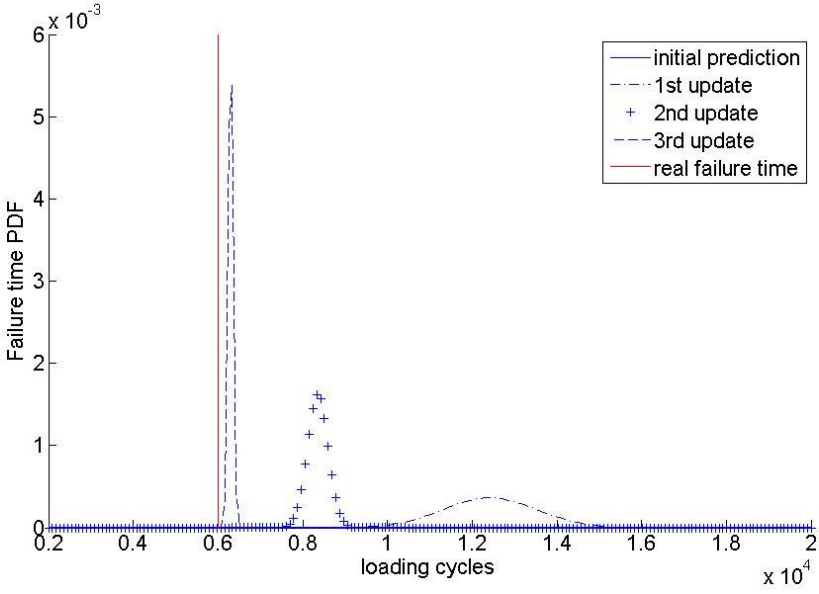

Fig. 12 Distributions of predicted failure time for path #6

5 Comparative study and validation using ILI/NDE field data

In this section, a comparative study is performed between the proposed integrated method and the existing physics-based method using the ILI/NDE field data supplied by a Canadian pipeline operator. In addition, the performance of the proposed method under different ILI tool accuracy is also studied. A summary of the pipe properties and the flaw measured properties are given in the following Tables 13 and 14:

Table 13 Pipe properties

Property	Value
Diameter	863.6mm (34in.)
Nominal Wall Thickness	7.1mm (0.281in.)
Grade	X52
MOP	4.5MPa (649psi)

Table 14 Flaw measured properties

Date of Size	Growth Length	Peak Depth
February 2002	150mm (5.9in.)	2.95mm (0.116in.)
April 2007	150mm (5.9in.)	6.40mm (0.252in.)

5.1 Pressure data processing using rainflow counting

Pressure cycling drives pipe fatigue crack growth, and pressure data is used to calculate the SIF values. Fig. 13 is a plot of the pressure data from February 6, 2003 to March 31, 2007. It can be seen that the pipeline operations change in November 2005, and the pressure cycling also changes at that time. The rainflow-counting method is used to count the number of discrete pressure cycling ranges, which will subsequently be used in pipe stress analysis. Two output matrices, namely matrix 1 and matrix 2, are generated. Matrix 1 contains information for each individual cycle including cycle number, time information, and range of pressure. Matrix 2 organizes the individual cycles into different range limits, with the range increment set to 5 psi (0.034MPa). The rainflow-counting result is shown in Fig. 14. As can be seen, there are a large number of small cycles with small pressure ranges, and a small number of large cycles.

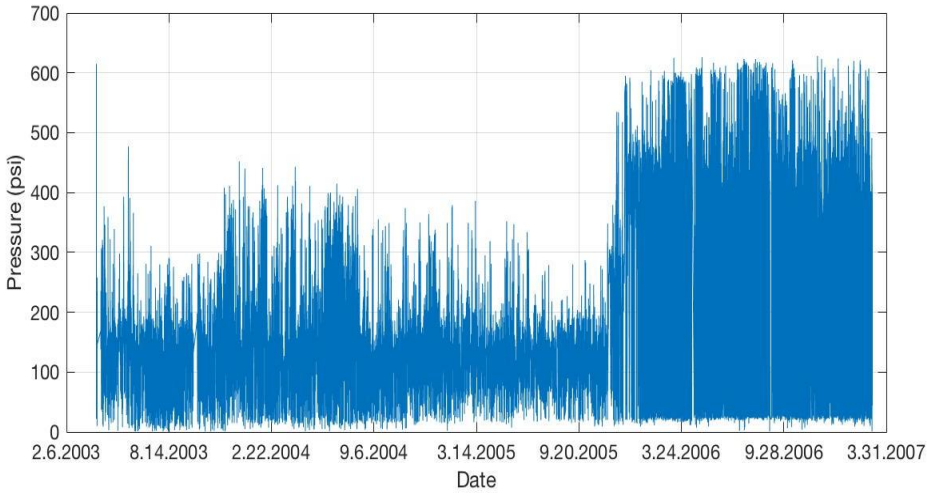

Fig. 13 Total pressure data from February 6, 2003 to March 31, 2007

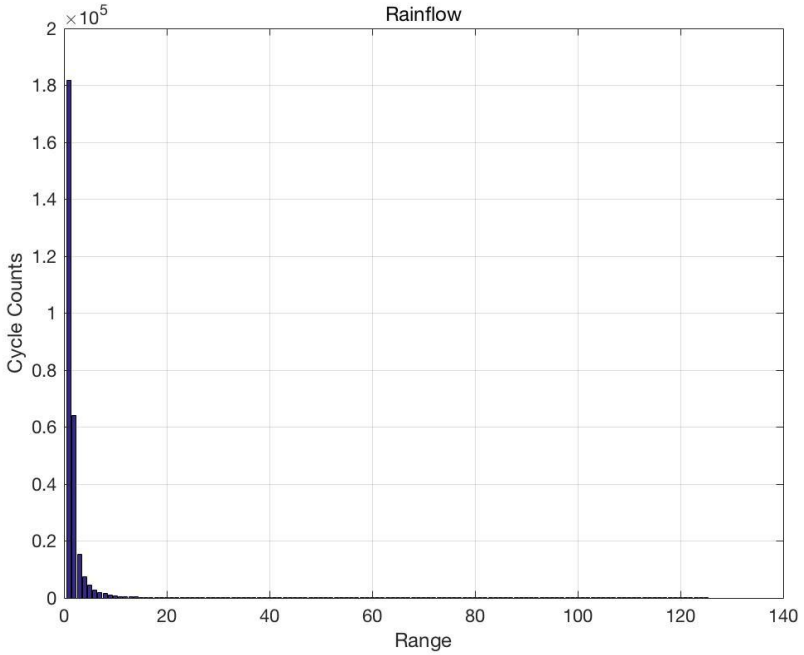

Fig. 14 Rainflow-counting result

5.2 Fatigue crack propagation based on the rainflow-counting results

As mentioned in the previous subsection, we can obtain two different output matrices from the rainflow-counting method, namely matrix 1 and matrix 2. The two matrices are based on the pressure data from February 6, 2002 to March 10, 2007. It is assumed that prior to February 6, 2003, the pressure data is the same from 2003-2004 since the operation had been the same during the period. It is obvious that matrix 1 should give more accurate results than matrix 2, but can be more computationally intensive to use to calculate fatigue crack propagation. Fig. 15 shows degradation paths generated using matrix 1 and the FE method. By using matrix 2, the pressure ranges can

be ranked in an increasing or decreasing order. Depending on the order, the upper bound or the lower bound can be used to represent each range limit. The investigations show that using matrix 2 by ordering the pressure ranges increasingly or decreasingly give very close degradation path results. It can also be found that matrix 1 and matrix 2 give relatively close crack depth values on both February 6, 2003 and Mar. 10, 2007.

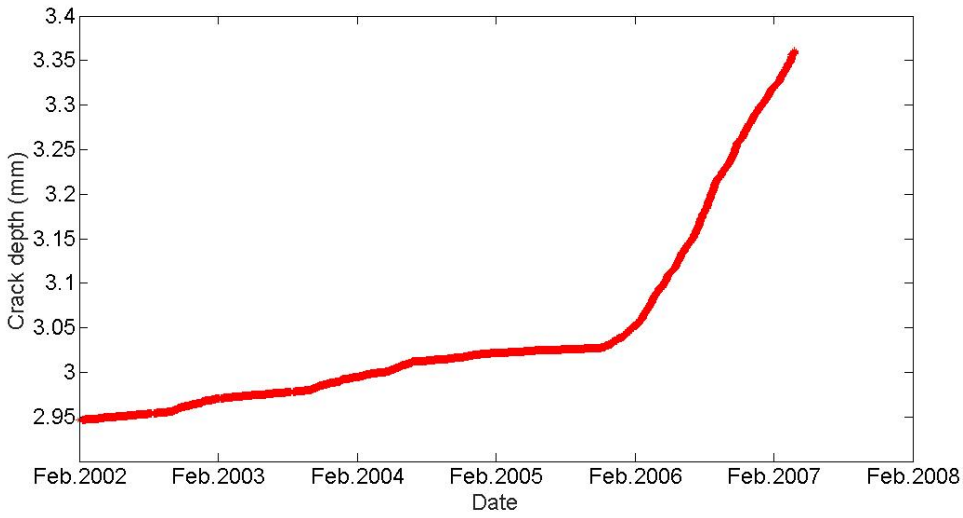

Fig. 15 Degradation paths generated using matrix 1

5.3 Critical crack depth determination

Once the critical crack size is reached, the pipe is considered failed, and thus the failure time and the remaining useful life can be determined. The critical flaw size depends on the nominal stress, the material strength, and the fracture toughness. The relationship between these parameters for a longitudinally oriented defect in a

pressurized cylinder is expressed by the NG-18 “ln-secant” equation [26]:

$$\frac{C_V \pi E}{4 A_C L_e \sigma_f^2} = \ln\left[\sec\left(\frac{\pi M_S \sigma_H}{2\sigma_f}\right)\right] \tag{21}$$

where

$$M_S = \frac{1-\frac{a}{tM_t}}{\frac{a}{t}} \tag{22}$$

$$M_t = [1+0.6275z-0.003375z^2]^{\frac{1}{2}},\ z=\frac{L_e^2}{Dt} \le 50 \tag{23}$$

$$\text{or} \quad M_t = 0.032z+3.3,\ z>50 \tag{24}$$

The values used in the equations are further explained as follows.

a is flaw depth;

t is the pipe wall thickness, and t=7.1mm(0.281in.);

E is the elastic modulus, and E=206GPa;

L_e is an effective flaw length, equal to the total flaw length multiplied by π/4 for a semi-elliptical flaw shape common in fatigue. In our study, $L_e=150\times\frac{\pi}{4}$=117.8mm;

σ_f is the flow stress typically taken as the yield strength plus 68MPa, or as the average of yield and ultimate tensile strengths. $\sigma_f=\sigma_y$+10=403+68=471MPa(68.42ksi);

σ_H is the nominal hoop stress due to internal pressure. $\sigma_H=p\times\frac{D}{2t}$;

C_V is the upper shelf CVN impact toughness. C_V=4.9m·kg (35.8ft·lbs);

A_c is the cross-sectional area of the Charpy impact specimen. A_c=80mm^2(0.124 in.^{2}).

The field data is applied to these equations, and the resulting relationship is shown in Fig. 16. Given the crack length of 150mm (5.9in.), if the internal pressure is equal to the Maximum Operating Pressure (MOP) of 4.5MPa (649psi), the critical depth-to-thickness ratio will be 0.6688. Thus, the critical crack depth is 0.6688×7.1=4.8mm (0.188 in.). The discrepancies from the NDE depth in April, 2007 (6.4mm) is because this way to determine the critical depth is relatively conservative.

5.4 ILI-NDE depth distribution

NDE fatigue crack depth is considered as accurate for the purposes of this case study. ILI-NDE depth data give the differences between the collected ILI depth values and the corresponding NDE depth values, and thus can represent the accuracy of the ILI tool in measuring fatigue crack depth. With all the 16 sample field depths provided by the industry partner, a normal distribution is used to fit the ILI-NDE depth data, with the estimated mean 0.6669 mm (0.026 in.), and standard deviation 0.4795 mm (0.0189 in.).

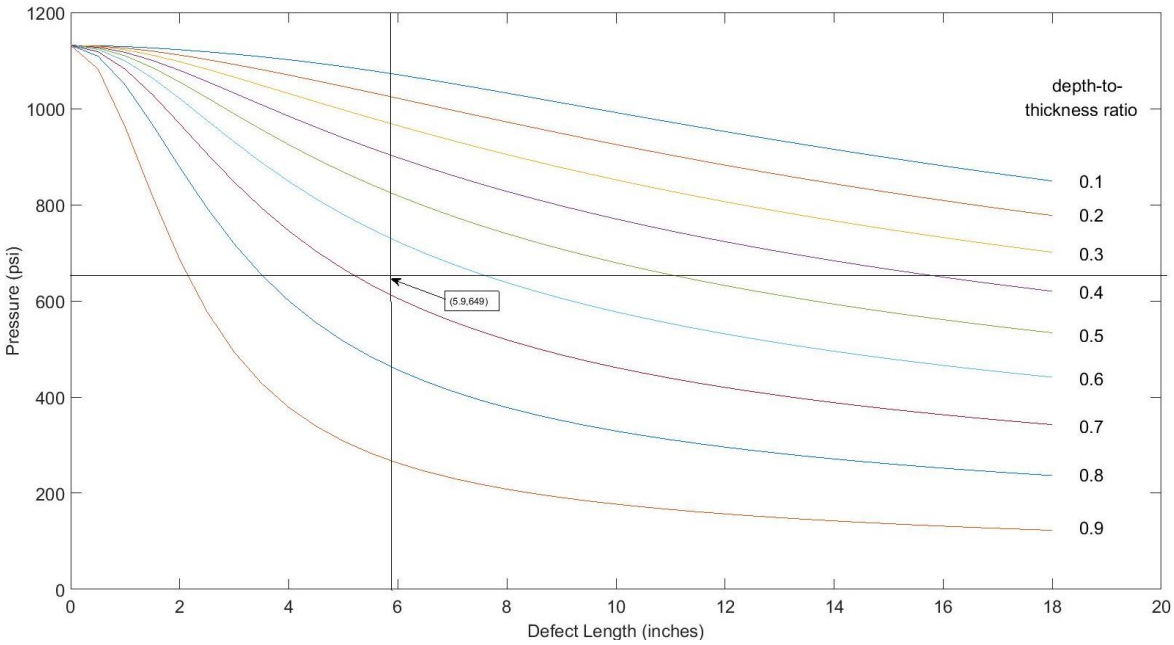

Fig. 16 Relationship between failure stress and flaw size

5.5 Limitations of the existing physics-based method

The fatigue crack growth results by the existing physics-based method are briefly discussed in Section 5.2 and presented in Fig. 15. With the physics-based method based on the Paris' law, fixed model parameters are used: m=3 and C=3.0×10^{-20}MPa$\sqrt{\text{mm}}$ (8.6×10^{-19}psi$\sqrt{\text{in}}$). The finite element method and Raju and Newman method are employed in stress intensity factor calculations. As can be seen in Fig. 15, the crack depth in April 2007 is 3.37mm (0.1325 in.), which is far from the actual crack depth of 6.40mm (0.252 in.) which is measured using the NDE tool. The crack growth results show that the existing physics-based method does not perform well in this case study. However, physics-based methods are were much better aligned to

observed growth using more common conservative industry approaches to calculate SIF such as BS 7910 and API 579.

5.6 The integrated method and its performance under different ILI tool accuracy

With this dataset, 2 NDE measurements are available, and are used to find the real *m* value by trying different *m* values. It is found that an m value of 3.11 will give the crack depth of 0.252 inch in April 2007, meaning that 3.11 is the real *m* value for the pipe. The crack growth curves for *m*=3.11 and *m*=3 are shown in the following figure, Fig. 17. With the real *m* value, the real crack depth value can be obtained at any given point in time.

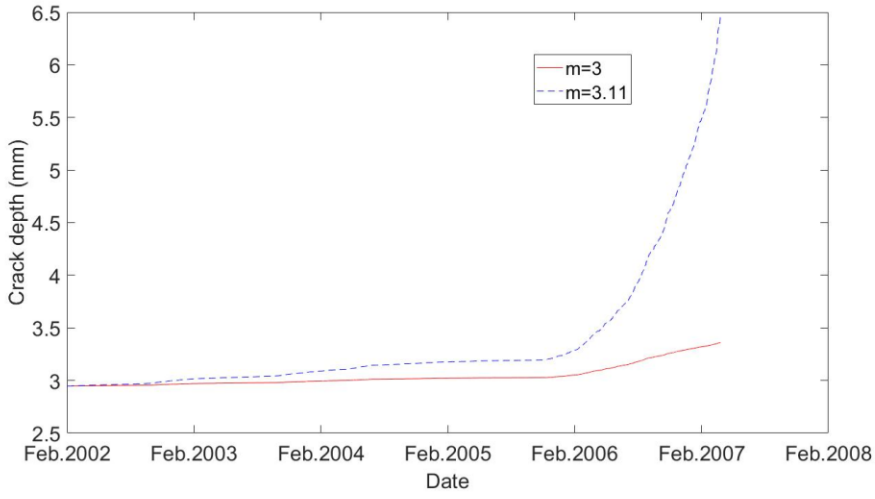

Fig. 17 Real crack growth curve

The prediction performance of the proposed integrated method is investigated

under different ILI tool accuracy, measured by the ILI tool measurement uncertainty. In this section, we investigate the integrated method's performance when the ILI tool measurement uncertainty standard deviation is equal to 0.25mm (0.01in.), 0.38mm (0.015in.), and 0.50mm (0.02in.), respectively.

Feb. 2002 is set as the starting point for crack growth, where the crack depth is 2.95mm (0.116in.). Jun. 2006 is used as the first inspection point because ILI data is available from that time. Nov. 2006 is used as the second inspection point. The crack depth will be predicted for Apr. 2007, and compared with the NDE depth measurement of 6.40mm. As can be seen from the real crack growth curve shown in Fig. 17, the real crack depth is 3.96mm in Jun. 2006 and 5.13mm in Nov. 2006. The first case that was investigated was when the ILI measurement uncertainty standard deviation is 0.25mm. To try to fully assess the prediction performance of the integrated method for the Jun. 2006 inspection point, five ILI data points were sampled from a normal distribution with a mean of 3.96mm (real crack depth) and standard deviation of 0.25mm. For each of the sampled ILI data points, parameter *m* is updated using Bayesian inference, and the mean of the five updated *m* values is 3.129 for Jun. 2006, as shown in Table 15. The same approach is done for the Nov. 2006 inspection point, and the mean of the updated *m* value is 3.101. The mean predicted crack depth values for Apr. 2007 are also obtained and recorded in Table 15(1). As can be seen, the updated *m* value gets closer to the real m value of 3.11, and the predicted crack depth for Apr. 2007 gets closer to the real crack

depth 6.40mm.

Next we investigate the cases where the ILI tool measurement uncertainty standard deviation is equal to 0.38mm and 0.50mm. The same procedure as mentioned above is followed, and the results are recorded in Table 15(2) and 15(3). From the results in Table 15, it can be seen that the best prediction performance is achieved when the measurement uncertainty is the smallest (0.25mm), and the prediction performance becomes worse when the measurement uncertainty is larger, as expected. It can also be observed that for all three ILI measurement uncertainty cases, the integrated method outperforms the existing physics-based method. Note that for the "ILI-NDE Depth sample" data, the ILI tool measurement uncertainty standard deviation is 0.48mm, which is between the case (Std.=0.38) and the case (Std.=0.50). It is expected that the ILI tool accuracy will keep improving in the future, which will result in more accurate predictions of crack depth using the integrated method.

Table 15 Update results

(1) σ_{ILI}=0.25mm

Inspection year	Feb. 2002	Jun. 2006	Nov. 2006
Crack depth(mm)	2.95	3.96	5.13
Mean of m	3	3.129	3.101
Std of m	0.15	0.019	0.008
Predicted crack depth for Apr. 2007	3.37	Reaching 6.40mm in Dec. 2006	5.64

(2) σ_{ILI}=0.38mm

Inspection year	Feb. 2002	Jun. 2006	Nov. 2006
Crack depth(mm)	2.95	3.96	5.13
Mean of m	3	3.097	3.098
Std of m	0.15	0.054	0.018
Predicted crack depth for Apr. 2007	3.37	5.23	5.31

(3) σ_{ILI}=0.50mm

Inspection year	Feb. 2002	Jun. 2006	Nov. 2006
Crack depth(mm)	2.95	3.96	5.13
Mean of m	3	3.029	3.074
Std of m	0.15	0.106	0.042
Predicted crack depth for Apr. 2007	3.37	3.58	4.27

6 Conclusions

Managing fatigue cracks has been a top priority for liquid pipeline operators. Existing inline inspection tools for pipeline defect evaluation have fatigue crack measurement uncertainties. Furthermore, current physics-based methods are mainly used for fatigue crack growth prediction, where the same or similar fixed model parameters are used for all pipes. They result in uncertainty that requires a conservative approach for integrity management approach and management and risk mitigation strategies. In this paper, an integrated approach is designed to predict pipeline fatigue crack growth with the presence of crack sizing uncertainty. The proposed approach is carried out by integrating the physical models, including the stress analysis models, the damage propagation model governed by the Paris' law, and the ILI data. With the proposed integrated approach, the FE model of a pipe with fatigue crack is constructed. ILI data is applied to update the uncertain material parameters for the individual pipe being considered, so that a more accurate fatigue crack growth prediction can be achieved. The rainflow counting method is used to count the loading cycles for the proposed integrated method under time-varying operating conditions. Furthermore, we compare the proposed integrated approach with the existing physics based method using examples based on simulated data. Field data provided by a Canadian pipeline operator is also used to validate the proposed integrated approach. At the end, the

examples and case studies in this paper demonstrate the limitations of the existing physics-based method, and the promise of the proposed integrated approach for achieving accurate fatigue crack growth prediction as ILI tool measurement uncertainty further improves. Enbridge recently announced a multi-year collaboration agreement with NDT Global, to build a new generation of improved crack ILI to further improve measurement uncertainty [32]. The developed methods can contribute to a more efficient pipeline integrity management approach for managing crack threats by reducing unnecessary maintenance work and downtime.

Disclaimer: Any information or data pertaining to Enbridge Employee Services Canada Inc., or its affiliates, contained in this paper was provided to the authors with the express permission of Enbridge Employee Services Canada Inc., or its affiliates. However, this paper is the work and opinion of the authors and is not to be interpreted as Enbridge Employee Services Canada Inc., or its affiliates', position or procedure regarding matters referred to in this paper. Enbridge Employee Services Canada Inc. and its affiliates and their respective employees, officers, director and agents shall not be liable for any claims for loss, damage or costs, of any kind whatsoever, arising from the errors, inaccuracies or incompleteness of the information and data contained in this paper or for any loss, damage or costs that may arise from the use or interpretation of this paper.

References

[1] Canadian Energy Pipeline Association (CEPA), About Pipelines, Our Energy Connections, 2012.

[2] Mohitpour, M., Murray, A., McManus, M., and Colquhoun, I., 2010, Pipeline Integrity Assurance: A Practical Approach, American Society of Mechanical Engineers, New York.

[3] Zarea, M., Piazza, M., Vignal, G., Jones, C., Rau, J., and Wang, R., 2013, "Review of R&D In Support of Mechanical Damage Threat Management in Onshore Transmission Pipeline Operations," Proceedings of the 9th International Pipeline Conference, 2012, Vol. 2, AMER SOC MECHANICAL ENGINEERS, New York, USA, pp. 569–582.

[4] Pipeline Research Council International, 2014, Year in Review.

[5] Nielsen, A., Mallet-Paret, J., and Griffin, K., 2014, "Probabilistic Modeling of Crack Threats and the Effects of Mitigation," Proceedings of the Biennial International Pipeline Conference.

[6] Sutton, A., Hubert, Y., Textor, S., and Haider, S., 2014, "Allowable Pressure Cycling Limits for Liquid Pipelines," Proceedings of the Biennial International Pipeline Conference, IPC.

[7] Jardine, A. K. S., Lin, D., and Banjevic, D., 2006, "A Review on Machinery Diagnostics and Prognostics Implementing Condition-Based Maintenance," Mechanical Systems and Signal Processing, 20(7), pp. 1483–1510.

[8] Mansor, N. I. I., Abdullah, S., Ariffin, A. K., and Syarif, J., 2014, "A Review of the Fatigue Failure Mechanism of Metallic Materials under a Corroded Environment," Engineering Failure Analysis, 42, pp. 353–365.

[9] Zhao, F., Tian, Z., and Zeng, Y., 2013, "Uncertainty Quantification in Gear Remaining Useful Life Prediction Through an Integrated Prognostics Method," IEEE Transactions on Reliability, 62(1), pp. 146–159.

[10] Bott, S., and Sporns, R., 2008, "The Benefits and Limitations of Using Risk Based Probabilistic and Deterministic Analysis for Monitoring and Mitigation Planning," 2008 7th International Pipeline Conference, American Society of Mechanical Engineers, pp. 797–807.

[11] Hong, S. W., Koo, J. M., Seok, C. S., Kim, J. W., Kim, J. H., and Hong, S. K., 2015, "Fatigue Life Prediction for an API 5L X42 Natural Gas Pipeline," Engineering Failure Analysis, 56, pp. 396–402.

[12] Pinheiro, B. de C., and Pasqualino, I. P., 2009, "Fatigue Analysis of Damaged Steel Pipelines under Cyclic Internal Pressure," International Journal of Fatigue, 31(5), pp. 962–973.

[13] Oikonomidis, F., Shterenlikht, A., and Truman, C. E., 2014, "Prediction of Crack Propagation and Arrest in X100 Natural Gas Transmission Pipelines with a Strain

Rate Dependent Damage Model (SRDD). Part 2: Large Scale Pipe Models with Gas Depressurisation," International Journal of Pressure Vessels and Piping, 122, pp. 15–21.

[14] Oikonomidis, F., Shterenlikht, A., and Truman, C. E., 2013, "Prediction of Crack Propagation and Arrest in X100 Natural Gas Transmission Pipelines with the Strain Rate Dependent Damage Model (SRDD). Part 1: A Novel Specimen for the Measurement of High Strain Rate Fracture Properties and Validation of the SRDD Model Parameters," International Journal of Pressure Vessels and Piping, 105–106, pp. 60–68.

[15] Varela, F., Yongjun Tan, M., and Forsyth, M., 2015, "An Overview of Major Methods for Inspecting and Monitoring External Corrosion of on-Shore Transportation Pipelines," Corrosion Engineering, Science and Technology, 50(3), pp. 226–235.

[16] Bates, N., Lee, D., and Maier, C., 2010, "A Review of Crack Detection in-Line Inspection Case Studies," 2010 8th International Pipeline Conference, American Society of Mechanical Engineers, pp. 197–208.

[17] Slaughter, M., Spencer, K., Dawson, J., and Senf, P., 2010, "Comparison of Multiple Crack Detection in-Line Inspection Data to Assess Crack Growth," 2010 8th International Pipeline Conference, American Society of Mechanical Engineers, pp. 397–406.

[18] Wang, H., Yajima, A., Y. Liang, R., and Castaneda, H., 2015, "A Bayesian Model Framework for Calibrating Ultrasonic in-Line Inspection Data and Estimating Actual External Corrosion Depth in Buried Pipeline Utilizing a Clustering Technique," Structural Safety, 54, pp. 19–31.

[19] Zhao, F., Tian, Z., Bechhoefer, E., and Zeng, Y., 2015, "An Integrated Prognostics Method under Time-Varying Operating Conditions," IEEE Transactions on Reliability, 64(2), pp. 673–686.

[20] Roshanfar, M., and Salimi, M. H., 2015, "Comparing of Methods of Cycle Calculating and Counting to the Rain Flow Method."

[21] NIST, Materials Reliability Division, 2007, "Mechanical Properties and Crack Behavior in Line Pipe Steels," DOT Quarterly Report.

[22] Al-Muslim, H. M., and Arif, A. F. M., 2010, "Effect of Geometry, Material and Pressure Variability on Strain and Stress Fields in Dented Pipelines under Static and Cyclic Pressure Loading Using Probability Analysis," Proceedings of the ASME International Pipeline Conference 2010, VOL 1, AMER SOC MECHANICAL ENGINEERS, New York, NY 10016-5990 USA, pp. 381–395.

[23] Silva, J., Ghaednia, H., and Das, S., 2012, "Fatigue Life Assessment for NPS30 Steel Pipe," Proceedings of the 9th International Pipeline Conference, AMER SOC MECHANICAL ENGINEERS, New York, NY 10016-5990 USA, pp. 619–624.

[24] Shim, D., and Wilkowski, G., 2014, "Bulging Factor for Axial Surface Cracks in Pipes."

[25] Newman, J., and Raju, I., 1981, "An Empirical Stress-Intensity Factor Equation for the Surface Crack," Engineering Fracture Mechanics, 15(1–2), pp. 185–192.

[26] Michael Baker Jr., 2004, OPS TTO5 – Low Frequency ERW and Lap Welded Longitudinal Seam Evaluation.
[27] Chookah, M., Nuhi, M., and Modarres, M., 2011, “A Probabilistic Physics-of-Failure Model for Prognostic Health Management of Structures Subject to Pitting and Corrosion-Fatigue,” Reliability Engineering & System Safety, 96(12), pp. 1601–1610.
[28] Jin, Q., Sun, Z., and Guo, W., 2014, “Experimental and Finite Element Study on the Fatigue Growth of a Semi-Elliptical Surface Crack in aX80 Pipeline Steelspecimen,” Advances in Civil and Industrial Engineering Iv, G. Li, C. Chen, B. Jiang, and Q. Shen, eds., pp. 3026–3029.
[29] Carpinteri, A., and Brighenti, R., 1998, “Circumferential Surface Flaws in Pipes under Cyclic Axial Loading,” Engineering Fracture Mechanics, 60(4), pp. 383–396.
[30] Carpinteri, A., 1993, “Shape Change of Surface Cracks in Round Bars under Cyclic Axial Loading,” International Journal of Fatigue, 15(1), pp. 21–26.
[31] Zhao, F., Tian, Z., and Zeng, Y., 2013, “A Stochastic Collocation Approach for Efficient Integrated Gear Health Prognosis,” Mechanical Systems and Signal Processing, 39(1–2), pp. 372–387.
[32]https://www.ndt-global.com/news/enbridge-partnership-to-advance-pipeline-technology-innovation